Ultracompact Retrodirective Antenna Arrays With Superdirective Radiation Patterns

Ultra-Compact Retrodirective Antenna Arrays with Superdirective Radiation Patterns

Oleksandr Malyuskin, Vincent Fusco, *Fellow, IEEE*

***Abstract*— It is shown that the Direction-of-Arrival (DoA) information carried by an incident electromagnetic wave can be encoded into the evanescent near field of an electrically small antenna array with a spatial rate higher than that of the incident field oscillation rate in free space. Phase conjugation of the received signal leads to the retrodirection of the near field in the antenna array environment which in turn generates a retrodirected far-field beam towards the original DoA. This electromagnetic phenomenon enables electrically small retrodirective antenna arrays with superdirective, angular super-resolution, auto-pointing properties for an arbitrary DoA. Theoretical explanation of the phenomenon based on first principle observations is given and full-wave simulations demonstrate a realisability route for the proposed retrodirective terminal that is comprised of resonance dipole antenna elements. Specifically it is shown that a 3-element disk-loaded retrodirective dipole array with 0.15λ spacings can achieve 3.4dBi maximal gain, 3dBi front-to-back ratio and 13% return loss fractional bandwidth (at 10dB level). Next it is demonstrated that the radiation gain of a 3-element array can be improved to approximately 6dBi at expense of the return loss fractional bandwidth reduction (2%).**

***Index Terms*— Antenna array, diffraction limit, dipole antennas, directive antennas, electromagnetic coupling, near field, radiation pattern, wireless communications**

I. Introduction

ANTENNA terminals are widely used in wireless communication systems e.g. for point-to-point mobile communications and sensor networking [1], [2]. Commonly these antenna terminals generate an omnidirectional radiation pattern in order to ensure complete spatial coverage for signal reception and/or transmission. An omnidirectional radiation pattern in receive mode is essential in non-steered systems for signal reception from an arbitrary direction of arrival (DoA). However in the transmission mode a narrow beam pattern radiated towards the communicator by the antenna terminal would add significant benefits to a communication, [1, 2] or wireless energy transfer system, [3]. Namely, higher directivity of the antenna system towards the intended receiver reduces the energy loss associated with the electromagnetic (EM) radiation in unwanted directions, increases signal-to-noise ratio at the receiver for the same transmitter input power [2], [4] and also can minimize multipath effects. Ultimately these features lead to lower bit error rate (BER) of the received signal and reduction of electromagnetic pollution through reduced EIRP and spatial radiation control.

A number of antenna solutions exist for relatively compact directive antenna terminals [5], [6]. Probably the most famous is the Yagi-Uda antenna [7], [8] which belongs to the class of endfire radiating antenna arrays [5], [9]. Other examples include high gain endfire radiating arrays based on electrically small resonant antenna elements separated by approximately one tenth of the radiation wavelength λ [9], [10]. Of course with these arrangements omnidirectional signal coverage is sacrificed since high gain can only be obtained in a preferred direction in space along the array axis.

To meet the requirement of full azimuthal plane coverage, electronically steerable antennas based on two-dimensional arrays, particularly circular antenna arrays with a characteristic radius of quarter- to half-wavelength of radiation have been proposed [11], [12]. Electronic beam scanning in the horizontal plane of a circular array can be realized by array phasing, switched array steering [11] or by varying the reactive loading across the terminals of passive antenna elements as in electronically steerable passive array radiator (ESPAR) antennas [12], [13]. ESPAR antennas normally employ dipole or monopole antenna passive elements with typically quarter-wavelength separation configured in a circular array with an active central element. Electronically steerable antenna arrays open up many new possibilities, including directional beam scanning, lowering the received signal BER and jamming interference reduction, [14]. However the electronic scanning in these antennas is based on heavy digital processing which needs inputs related to the DoA, channel/propagation environment dynamic characterization, etc., [14], [15].

In this paper we propose a fundamentally new class of small antenna terminals with automatic reconfigurable DoA dependent superdirective radiation pattern based on the principle of signal phase conjugation, [16]. Here the term "superdirective" refers to the antenna array radiation pattern which overcomes the Raleigh angular resolution limit [17]

$$\theta_A \approx \lambda / L_A, \tag{1}$$

where L_A is the antenna array aperture size.

This work was supported by the Leverhulme Trust, UK through the Grant RPG-2013-117. The authors are with The Institute of Electronics, Communications and Information Technology, Queen's University Belfast, Belfast, BT3 9DT, U.K.

(e-mail: o.malyuskin@qub.ac.uk; v.fusco@ee.qub.ac.uk)

It is well known that phase conjugation, PC, of the incoming signal wavefront forms the basis of retrodirective antenna arrays operation [16], [18]. Such arrays automatically retro-direct an incoming signal towards the original source without *a priori* knowledge of its spatial location [16], [18], [19]. Previously it was shown that retrodirective arrays can be used for full-duplex wireless communications as well as for efficient wireless energy transfer [3], [16], [18], [19] where the tasks like DoA estimation, target tracking, beam pointing and carrier recovery are based entirely on analog circuitry [16], [19]. Analogue signal processing has several distinct advantages over the digital-based counterpart, namely lower power consumption, high-speed tracking in real time and high sensitivity to low-power signals [16].

Traditionally retrodirective antenna arrays are constructed by merging standard antenna arrays with dedicated electronic circuitry performing PC [16], [20]. The elements in conventional narrowband resonant antenna arrays are normally spaced at around the half-wavelength of radiation [21], with the aim to reduce mutual coupling and enhancing the directivity of the array without appearance of grating lobes. As is well known reduction of radiating element spacing leads to higher intensity of the EM near field components (reactive EM field) which results in higher mutual coupling, widely considered as a primary source of antenna array performance degradation [21], [22]. While in general this is true since the increased reactive field leads to smaller frequency bandwidth, lower radiation resistance, reduced efficiency and mismatch of the antenna elements [5], the beneficial aspects of the reactive EM field in antenna environment has not received substantial attention.

Importantly, this paper will offer the first demonstration that DoA information can be encoded in the near field of the dense antenna array with much higher spatial rate than it is possible with a conventional array composed of half-wavelength spaced elements. This can be understood by expanding the array scattered field into its plane wave spectrum where evanescent harmonics with fast spatial oscillation contribute dominantly into the Fresnel and quasistatic near field, [23], [24]. A crucial feature of the dense retrodirective array operation will be demonstrated, namely that phase conjugation of the voltage induced across the antenna array terminals not only leads to the retrodirection of the propagating part of the field but also to the retrodirection of the reactive (oscillating) EM field [25]. Consequently the retrodirected field in the array environment generates the transmission-mode array excitation vector (amplitudes and phases of voltages across the antenna array terminals) such that the array radiates a directive beam back along the DoA with angular bandwidth overcoming the Raleigh angular resolution limit (1).

Realization of this angular super-resolution scenario requires high intensity of the evanescent field in the array environment exceeding the magnitude of the incident field in order to efficiently encode the DoA information into the highly-oscillatory evanescent harmonics. This is only possible when the antenna elements operate in EM resonance leading to high electric currents generating large scattered field. Usually, the EM resonance of the electrically small antenna elements in free space can be achieved by inductive lump loading, folding and spatial antenna loading using, e.g. top caps [5],[6], [9], [10]. In this paper we study a compact retrodirective array formed by a number of densely packed hat-loaded dipole antennas, however the angular super-resolution phenomenon can be realized in any compact (electrically small) resonance antenna array regardless of the antenna elements type.

It should be noted that the proposed retrodirective array can be classified as an angular super-resolution array and is different from the classical superdirective arrays composed of isotropic radiators [26]. The major difference is that in classical superdirective arrays the excitation vector values are the roots of the array polynomial. In the case we present here of a retrodirective array composed of resonant antenna elements the excitation vector is set by the superposition of the incident plane wave and the scattered field in the array environment which, in essence, is analogous to the super-resolution filter function [27].

The rest of the paper is organized as follows. Section II outlines the principle of operation of the proposed retrodirective array composed of densely packed hat-loaded dipole antennas. The EM resonance role in the retrodirected beam generation is emphasized and the antennae parameters are briefly discussed. Next, in Section III the mechanism for EM field retrodirection by a couplet or triplet of isotropic radiators and resonant antenna elements is discussed in detail. This study forms a basis for the analysis of the antenna arrays with different lattice arrangements. In Section IV a parametric study of array performance is carried out. Finally in Section V the conclusions are summarized. The relevant mathematical derivations are detailed in the Appendix.

II. Principle of Operation

Consider a compact retrodirective N-element antenna array, Fig. 1, illuminated by a signal EM plane wave (PW) with monochromatic, $\exp(-i\omega t)$, frequency carrier.

In the rest of this paper compactness of the array will be taken to mean that its characteristic spatial footprint size D_a does not exceed a radiation half-wavelength,

$$D_a \le \lambda/2 \tag{2}$$

The array is composed of electrically small resonant antenna elements [10] with characteristic size a satisfying the condition $k_0 a \approx 1$, where the wavenumber $k_0=2\pi/\lambda$. This condition is less stringent than the criterion $k_0 a << 1$ adopted for single classical electrically small antennas [28], however it should be noted that arrays of small antenna elements are studied in this paper therefore the classical requirement $k_0 a << 1$ needs to be relaxed. The analysis developed in this paper can be applied to arrays composed of any type of antenna element, however for the brevity's sake small resonant antennas realized as top-loaded dipoles are considered.

Consider now retrodirective antenna terminal action as follows.

A. Signal reception

The incident PW induces current distributions $I_n(z)$ along each of the antenna elements, n =1,2,…N is the antenna element index number. These antennae currents contain the signal PW direction of arrival (DoA) information encoded with high spatial frequency sampling rate due to the fact that the antenna elements located in the near field of each other.

To illustrate this statement further, the phase difference between the voltages across the antenna terminals T_1, T_2 and T_3 in the 3-element array arranged in the equilateral triangular lattice, Fig.1(a), are calculated using the full-wave electromagnetic solver FEKO (www.feko.info).

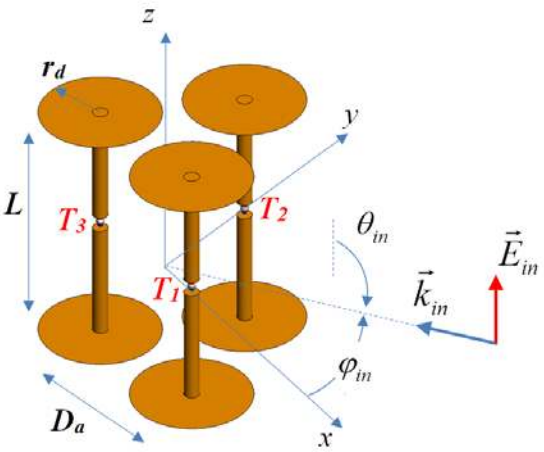

(a)

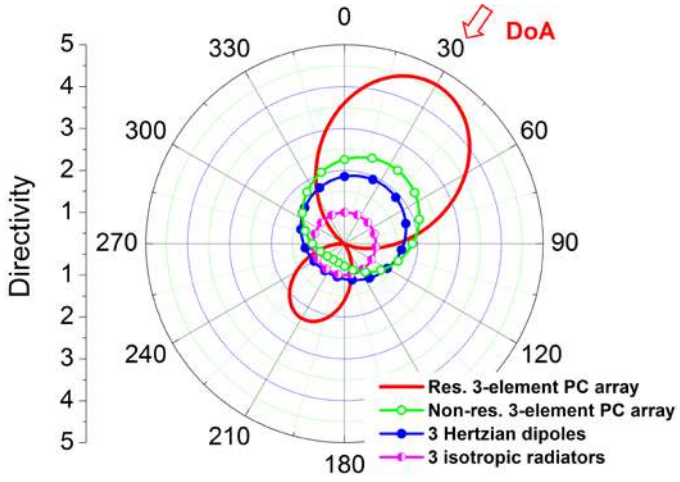

(b)

Fig.1. Compact retrodirective antenna array illuminated by a monochromatic PW. Fig.1(a), the antenna elements are electrically small resonant antennas oriented along the z axis and can be arbitrarily distributed in the horizontal xy plane. The phase of the incoming PW is conjugated at the antenna terminals T_1-T_3 which leads to the generation of a superdirective radiation pattern in the transmission mode with maximum directivity back along the DoA. In Fig.1(b) the radiation patterns of 3 Hertzian dipoles and 3 spherical wave sources with excitation phases $(-\varphi_1, -\varphi_2, -\varphi_3)$, φ_i is the phase of the incident PW in free space at the position of the i-th element center, are presented together with the PC array data. The radiation patterns of both the resonant (red solid line) and non-resonant (green line with hollow dots) PC arrays are shown for comparison.

The inter-element spacings used are 0.15λ, the length of each dipole antenna is 0.25λ, top disk radius 0.06λ (λ is chosen to be 0.125m at 2.4GHz). The array is illuminated by a monochromatic PW in the horizontal plane

$$\vec{E}_{in}(\vec{r}) = \vec{e}_{in}\exp\left(i\vec{k}_{in}\cdot\vec{r}\right) \tag{3}$$

with unit polarization vector along the z axis, $\vec{e}_{in} = \vec{z}_0$, and the wavevector $\vec{k}_{in}$

$$\vec{k}_{in} = k_0\left(\vec{\kappa} + \vec{z}_0\cos\theta_{in}\right) \tag{4}$$

where $\vec{\kappa} = (\cos\varphi_{in}, \sin\varphi_{in}, 0)$ is the incident wavevector projection onto the horizontal plane, θ_{in}, φ_{in} are the elevation and azimuthal incidence angles correspondingly.

In Fig. 2 the phase differences $\Delta\varphi_{Tm-Tn}$ between the voltages across the terminals m and n, (m, n=1,..,3) are calculated along with the phase difference of the incident field in the positions $\vec{\rho}_m$, (m=1,2,3), corresponding to the antenna element centers

$$\Delta\varphi_{12} = \vec{k}_{in}\cdot(\vec{\rho}_2 - \vec{\rho}_1), \quad \Delta\varphi_{23} = \vec{k}_{in}\cdot(\vec{\rho}_3 - \vec{\rho}_2), \ldots \tag{5}$$

It can be seen from Fig. 2 that the phase difference between the voltages across the antenna terminals varies significantly, on average several times larger than the phase difference of the incident EM field at the location of the corresponding antenna centers positions without the array present. This effect occurs due to strong near field EM coupling between the resonance antenna elements and from the viewpoint of the PW spectral representation can be considered as an array effective area expansion [29].

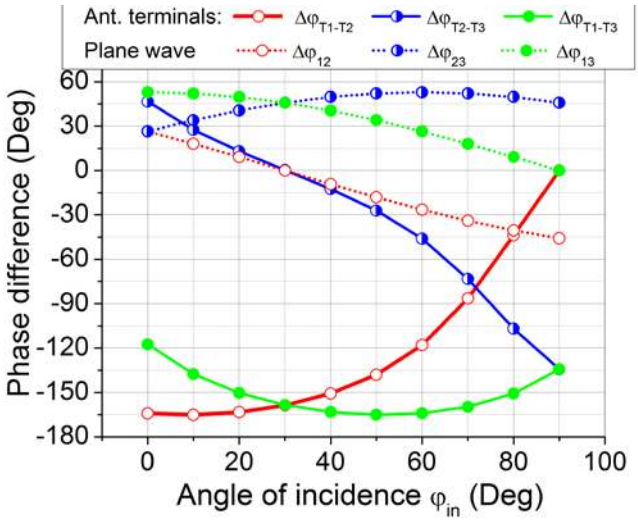

Fig.2. Voltage phase difference induced by the incident plane wave across the antenna terminals in Fig.1a, T_1-T_3, solid lines, and the phase difference of the incident field in the positions corresponding to the antenna element centers, dotted lines with the array removed. Plane wave is incident in the horizontal plane. The array is in receive mode.

This last point can be illustrated by the comparison of the

radiation patterns in the transmission (or retrodirection) mode, Fig.1(b), generated by the array of EM coupled resonance antennas, red solid line and by the array of three Hertzian point-like dipole sources not EM coupled to each other, blue line with hollow markers. The array complex-valued excitation vector (a_1, a_2, a_3) consists of the complex conjugate voltages $\left(v_1^*, v_2^*, v_3^*\right)$ induced across the antenna terminals T_1-T_3 in case of the resonant array and conjugate incident field phasors (exp -$i\varphi_1$, exp -$i\varphi_2$, exp –$i\varphi_3$), where $\varphi_i = \vec{k}_{in} \cdot \vec{\rho}_i$, i = 1,2,3, in the case of the array of Hertzian sources. In both cases uniform amplitude excitation is applied, $|a_1|=|a_2|=|a_3|$. Fig.1(b) shows the radiation pattern for θ_{in} =0°, φ_{in} =30°. The angular bandwidth at 0.707 level is 68° for the resonant antenna array and 200° for the Hertzian dipole array, i.e. the near-field coupled array generates approximately a 3 times narrower beam as compared to the case when no EM coupling is present.

It is interesting to note that an endfire superdirective *line* array [26] composed of Hertzian dipole sources with excitation phases (0, 120°, 240°) and uniform 0.15λ spacing generates a beam with 66° angular bandwidth at 0.707 level, which is, approximately equal to the angular bandwidth of the resonant antenna array. It should be stressed again that the retrodirective array can steer the beam to any arbitrary azimuthal angle of arrival, unlike the endfire array, [9], [10], [26], which enables high gain only along one direction.

Let us now discuss in more detail retrodirection of the signal towards the intended communicator.

B. Signal retrodirection

Full-duplex wireless communications based on retrodirective arrays are discussed in [16], [19] and for efficient wireless energy transfer, [3]. The PC unit architecture for full duplex communications can be schematically represented by a diagram in Fig.3.

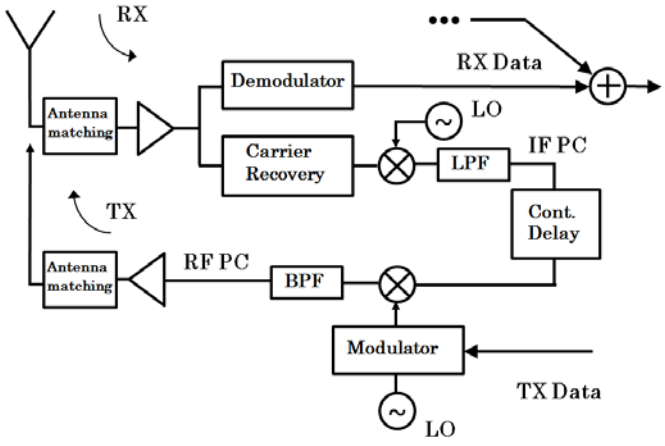

Fig.3. Schematic of phase conjugating full-duplex communication architecture.

In the receive (RX) chain the signal is split into the demodulator, where the RX digital data is recovered and the carrier recovery circuit which removes the modulation and extracts the RF carrier. The high-frequency RF carrier bearing the incident PW DoA information is mixed with a local oscillator (LO) signal and a resulting low-frequency PC signal at intermediate frequency (IF PC) is filtered by a low-pass filter (LPF). The IF PC signal can be delayed if required by controllable analog delay circuit. Next the IF PC signal feeds the transmit (TX) chain where it is mixed with a modulated TX data, up-converted and after passing a band-pass filter (BPF) re-applied to the same antenna terminal generating the retrodirected beam.

More detailed discussion on the realization of the PC circuitry can be found in review papers [16], [30]. Impedance matching between the antenna and PC circuitry is specific for each PC unit realization [16], [30], [31] but in general it is based on the conjugate matching technique [32]. It should also be noted that often the retrodirected signal has a small frequency offset with respect to the frequency of the incident wave carrier [16], [30]. From the mathematical point of view, the EM effect of the PC unit can be modelled in the transmit (TX) mode by numerical conjugation of the voltage phase across the n-th antenna terminals in the receive (RX) mode,

$$v_{nTX} = A_v v_{nRX}^* \tag{6}$$

where A_v is a real-valued number defined by the PC unit output power gain. Equation (6) was proven to be very accurate and in a very good agreement with the experimental data for high-quality PC units [16], [20].

III. Retrodirection of the EM Field

In this Section EM field retrodirection by a pair (couplet) and a triplet of PC scatterers is analyzed using the geometrical theory of diffraction in order to illustrate the EM retrodirection process of both propagating and evanescent EM field components. Then retrodirection by the arrays with more complex lattices is studied.

A. Propagating field retrodirection

Let us consider first the retrodirection of the incident propagating PW by a pair of point-like scattering centers, conjugating the incoming PW phase, Fig. 4(a). These centers can be represented by the isotropic radiators or Hertzian dipoles without EM coupling between them.

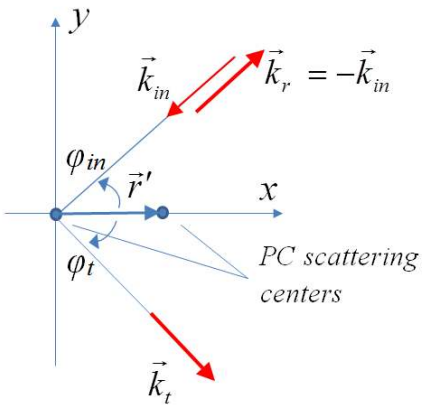

(a)

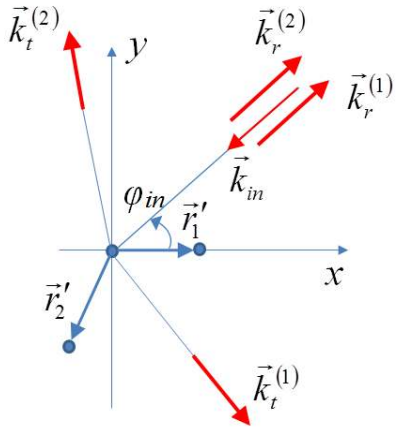

(b)

Fig.4. (a) Retrodirection and negative refraction of the incoming propagating PW by a pair of PC scattering centers; (b) spatial coherence of the retrodirected wave and incoherence of the negatively refracted partial waves in the arbitrary array geometry.

The incoming PW with a plane wave vector $\vec{k}_{in}$ gets phase conjugated at the PC scattering centers located at the origin of the coordinate system and also at the point with radius vector $\vec{r}'$, Fig. 4(a). The arising retrodirected wave $\vec{E}_{pc}(\vec{r})$ is formed by a superposition of the partial PC fields,

$$\vec{E}_{pc}(\vec{r}) \sim \sum_{\vec{r}'} \frac{\exp(ik_0 R)}{4\pi R} \exp\left(-i\vec{k}_{in} \cdot \vec{r}'\right) \tag{7}$$

where $R = |\vec{r} - \vec{r}'|$ and $\vec{r}$ is a radius-vector of the observation position. The maximum of the retrodirected field radiation pattern in the far field zone, $r >> r'$, occurs for the stationary phase point [24], [30] satisfying the condition

$$\nabla_{\vec{r}'}\left[ik_0\left(r - \vec{r}_0 \cdot \vec{r}' - \vec{k}_{in} \cdot \vec{r}'/k_0\right)\right] = 0 \tag{8}$$

where $\vec{r}_0 = \vec{r}/r$. In (8) an asymptotic expression

$$R = |\vec{r} - \vec{r}'| = \sqrt{r^2 + r'^2 - 2\vec{r} \cdot \vec{r}'} \approx r - \vec{r}_0 \cdot \vec{r}', \tag{9}$$

has been used. It can be seen that (8) is satisfied for an observation point with a radius vector $\vec{r}_0$ such that

$$\vec{r}_0 = -\vec{k}_{in}/k_0 \tag{10}$$

which gives a retrodirected wave for $y > 0$, Fig.4(a) with the wavefront normal vector

$$\vec{k}_r = -\vec{k}_{in} \tag{11}$$

For the scattering pair in Fig. 4(a) another solution satisfying (7) is possible in the $y < 0$ half-space with a radius vector

$$\vec{r}_0 = -\vec{\kappa} - |k_y/k_0|\vec{z}_0 \tag{12}$$

which corresponds to a negatively refracted wave with phase factor $\sim \exp\left(i\vec{k}_t \cdot \vec{r}\right)$. This wave propagates in the half-space $y < 0$ at the angle $\varphi_t = -\varphi_{in}$, i.e. in a mirror-symmetric direction with respect to the line connecting the scattering pair centers.

Importantly, for arbitrary array geometries (i.e. non-couplet arrangements) spatial coherence is preserved only for the retrodirected wave with $\vec{k}_r = -\vec{k}_{in}$. Spatial coherence for a negatively refracted wave occurs only for certain array geometries, like line or planar arrays [25]. In arbitrary three-dimensional geometries the negatively refracted partial fields are added incoherently. This scenario is illustrated in Fig. 4(b) for the case of a PC scattering triplet.

Now let us consider the case of resonance antenna elements with strong near field EM coupling. In this case the incident PW induces current distributions along the antenna elements $I_n(z)$, n =1,2,…with additional phase shift due to the near field coupling, and the retrodirected field will be given by a sum of partial waves

$$\vec{E}_{pc}(\vec{r}) \sim \sum_{\vec{r}'} A\left(\vec{k}_{in}, \vec{r}'\right) \frac{\exp(ik_0 R)}{4\pi R} \exp\left(-i\vec{k}_{res} \cdot \vec{r}'\right) \tag{13}$$

where the amplitudes $A\left(\vec{k}_{in}, \vec{r}'\right) \sim \int_{-L/2}^{L/2} I_n(z') \exp(ik_0 z') dz'$ and the wavevector $\vec{k}_{res}$ is represented by a sum of retrodirected wavevector $\vec{k}_r = -\vec{k}_{in}$ and additional vector $\vec{k}_c \sim \nabla_{\vec{r}'}\varphi$ proportional to the gradient of an additional phase shift φ due to antenna near field coupling , Fig.5(a),

$$\vec{k}_{res} = -\vec{k}_{in} - \vec{k}_c \tag{14}$$

As it has been shown earlier, Fig.2, in closely spaced resonant antennas the additional phase shift due to EM coupling is several times larger than the phase shift of the incident field in

the free space, therefore $\vec{k}_c \cdot \vec{r}' >> \vec{k}_{in} \cdot \vec{r}'$ for $\vec{r}' \neq 0$.

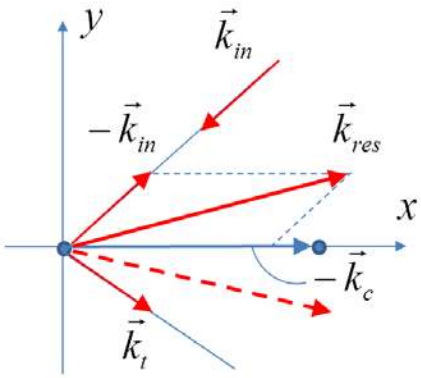

(a)

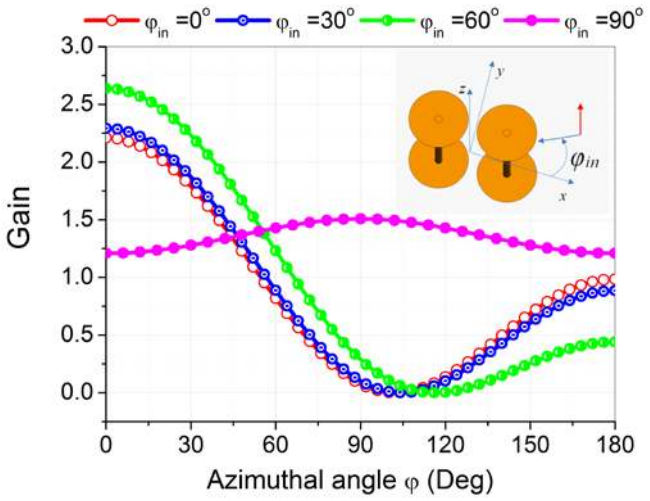

(b)

Fig.5. (a) Schematic representation of the retrodirected wave formation by a couplet of two resonant antennas, denoted by solid circles. (b) Full-wave simulation of the radiation pattern of two resonant disk-loaded 0.25λ-long dipole antennas separated by 0.15λ, λ=0.125m, with 10Ω matching load across the terminals. The pattern is symmetric in azimuthal plane with respect to φ=0 axis.

This results in a dominant endfire radiation by the couplet of resonance antennas, Fig.5(b), red to green lines, for any incidence angle φ_{in} except for φ_{in} =90°. For the incidence angle φ_{in} =90° a resonant antenna couplet radiates a broadside pattern, Fig.5(b), magenta line with solid circles. In Fig. 5(b) the gain radiation pattern is shown, defined in the normal way as the ratio of directivity to the radiation efficiency of the antenna system.

Propagating field retrodirection by the resonance antenna triplet is schematically shown in Fig. 6(a). If the spacings between the triplet antenna elements are approximately the same (more specifically of the same order), the additional wavevectors $\vec{k}_c^{(1)} \sim \nabla_{\vec{r}}\varphi_{12}$, $\vec{k}_c^{(2)} \sim \nabla_{\vec{r}}\varphi_{13}$ arising as a result of near field coupling are approximately symmetric with respect to the incident PW vector $\vec{k}_{in}$. Antenna elements are numbered from 1 to 3 as shown in Fig. 6(a).

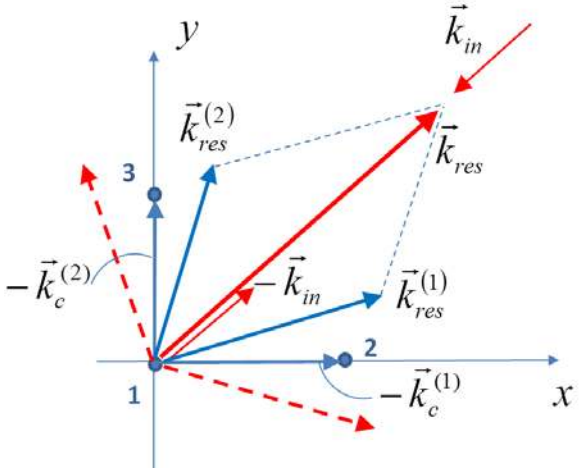

(a)

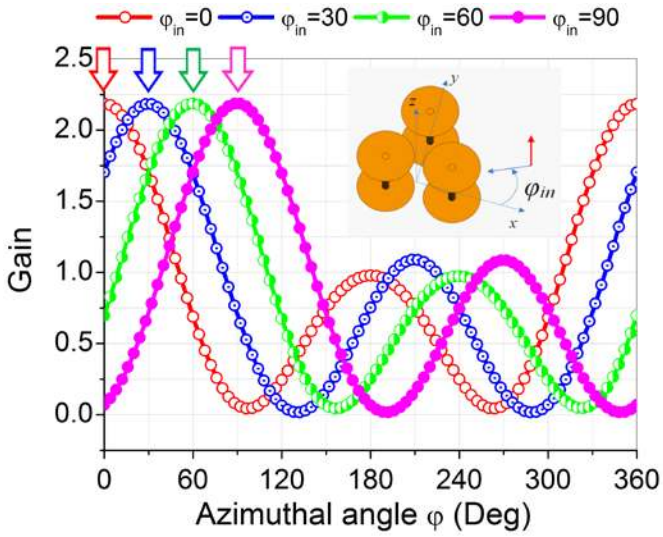

(b)

Fig.6. (a) Schematic representation of the retrodirected wave formation by a couplet of two resonant antennas, denoted by solid circles. (b) Full-wave simulation of the radiation pattern of three resonant disk-loaded 0.25λ-long dipole antennas in the equilateral triangular lattice with 0.15λ spacings, λ=0.125m, with 10Ω matching load across the terminals. The DoA angle is shown on the graph's top by an arrow of corresponding color.

If one of the spacings becomes much larger than the other one (more than 0.5λ), then dominant radiation will occur, in general into the endfire direction of the couplet with smaller inter-element distance. This situation will not be studied here in detail since we consider electrically small arrays with spacings not exceeding half-wavelength of radiation.

It is important to note that both the antennae currents phase shifts and amplitude weights $A\left(\vec{k}_{in}, \vec{r}'\right)$ are nonlinear functions of the antenna element spacings due to the non-linear spatial variation of the near field amplitude ~$1/r^2$, ~$1/r^3$ with distance r from the antenna. It is therefore advantageous to use antenna arrays that are arranged in equilateral triangular lattices or lattices with approximately equal spacings such that the additional phase vectors $\vec{k}_c$ are approximately symmetric with respect to the incident PW vector $\vec{k}_{in}$.

Full-wave simulation results shown in Fig.6(b) demonstrate that with a 3-element antenna array arranged in an equilateral triangular lattice retrodirection is possible for any arbitrary DoA angle in the azimuthal plane. The gain for the 3-element array with 0.15λ spacing is 3.4dBi, front to back ratio is ~3dBi. The half-maximum angular beamwidth is ~96° which is only marginally wider than the 90° angular bandwidth of the endfire superdirective line array of Hertzian dipoles with 0.15λ spacings with uniformly distributed roots of the array polynomial [26].

B. Retrodirection of the evanescent field in the antenna array environment

To get insight into the EM near field retrodirection in the PC antenna array environment the PW spectral expansion [23], [24] can be employed. The scattered/radiated by the array field in the receive or transmit (retrodirection) mode can be written as a superposition of the partial fields due to the antenna currents $I_n(z)$, $I_n^t(z)$,

$$\vec{E}_{sc(pc)}(\vec{r}) = \sum_{n=1}^{N} i\omega\mu_0 \left[\hat{I} + \frac{\nabla\nabla}{k_0^2}\right] \cdot \int_0^{L_n} \vec{z}_0 g(\vec{r},\vec{r}') I_n^{(t)}(z') dz' \quad (15)$$

where n is the antenna element number, N is a total number of antennas in the array , $I_n(z)$ and $I_n^t(z)$ are the current distributions in the receive and transmit (retrodirection) modes correspondingly and

$$g(\vec{r},\vec{r}') = \exp\left(ik_0|\vec{r}-\vec{r}'|\right)/4\pi|\vec{r}-\vec{r}'| \quad (16)$$

is a spherical wave function [30] and $\hat{I}$ is a unit dyad. Expanding the spherical wave function into the superposition of PWs with wavevectors $\vec{k} = (k_x, k_y, k_z)$

$$g(\vec{r},\vec{r}') = \frac{i}{8\pi^2} \int_{-\infty}^{\infty} \frac{\exp\left(i\vec{k}\cdot\vec{R}\right)}{\vec{k}\cdot\vec{z}_0} d\vec{\chi}, \quad (17)$$

where $\vec{\chi} = (k_x, k_y, 0)$, it is possible to obtain a representation of the scattered field in terms of propagating and evanescent PWs,

$$\vec{E}_{sc(pc)}(\vec{r}) \sim \sum_{n=1}^{N} \int_{-\infty}^{\infty} \vec{\mathrm{E}}(\vec{k}) \exp[i\vec{\chi}\cdot(\vec{\rho}-\vec{\rho}_n)] \exp(\pm ik_z z) \eta_n(\chi) d\vec{\chi} \quad (18)$$

where $\vec{\mathrm{E}}(\vec{k})$ are the spectral amplitudes, specified in Appendix B, $\vec{\rho}$ and $\vec{\rho}_n$ are the observation point radius-vector in the horizontal plane and the radius-vector of the n-th antenna element center position respectively and function $\eta_n(\chi)$ describes the spectral harmonics of the current distribution along the *n-th* antenna element,

$$\eta_n(\chi) = \int_0^{L_n} \exp(\mp ik_z z') I_n(z') dz' \quad (19)$$

In (18), (19) the upper sign is chosen when $z \geq z'$ and the bottom sign is chosen when $z \leq z'$.

The process of evanescent wave retrodirection can be considered in full analogy with the propagating PW case, Section III, A. However there are some differences, as explained below;

For clarity let us consider a partial evanescent PW $\sim \exp[i\vec{\chi}\cdot(\vec{\rho}-\vec{\rho}_n)]$ emanated from the isotropic source located at $\vec{\rho} = \vec{\rho}_n$. This partial PW excites the retrodirective center located at $\vec{\rho} = \vec{\rho}_j$, $j \neq n$, and gets its phase conjugated. As a result, two evanescent field components arise with spatial dependence

$$\vec{E}_{pc}(\vec{\rho}) \sim \exp[-i\vec{\chi}\cdot(\vec{\rho}_j - \vec{\rho}_n)] \exp[\pm i\vec{\chi}\cdot(\vec{\rho}-\vec{\rho}_j)], \quad (20)$$

where the attenuation factor exp(-|$k_z z$|) in the orthogonal to $\vec{\chi}$ direction is omitted. In (20) the factor $\exp[-i\vec{\chi}\cdot(\vec{\rho}_j-\vec{\rho}_n)]$ corresponds to the conjugated phase of the evanescent PW at the retrodirective center position $\vec{\rho} = \vec{\rho}_j$, the factor $\exp[+i\vec{\chi}\cdot(\vec{\rho}-\vec{\rho}_j)]$ corresponds to the partial evanescent wave "retrodirected" back towards the source at $\vec{\rho} = \vec{\rho}_n$ and factor $\exp[-i\vec{\chi}\cdot(\vec{\rho}-\vec{\rho}_j)]$ corresponds to the evanescent wave experiencing "negative refraction". The sign "+" appears in (20) as a result of the spectral decomposition reference axis inversion, [23]. Applying the stationary phase method to the spectral superposition composed of PWs (20) we can establish that maximum of the retrodirected field emitted by a source at $\vec{\rho} = \vec{\rho}_n$ occurs at the position

$$\begin{aligned} &\vec{\rho} = \vec{\rho}_n, \text{ retrodirected field} \\ &\vec{\rho} = 2\vec{\rho}_j - \vec{\rho}_n, \text{ negatively refracted field} \end{aligned}, \quad (21)$$

Negative refraction of the oscillating near field has been studied in detail in [25] for the line array geometry. In full analogy with the propagating PW case it can be shown that the spatial coherence in the arbitrary array geometry is only preserved for the retrodirected field, while "negatively" refracted spot can only be coherently formed in the lensing scenario with linear or planar retrodirective array [25].

Retrodirection of the near field has been numerically studied using a point-like Hertzian dipole located in number of positions in the vicinity (~0.2-0.4λ) of the 3-element PC array described earlier, Fig.7(a).

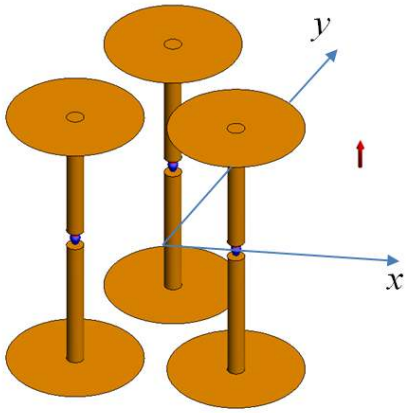

(a)

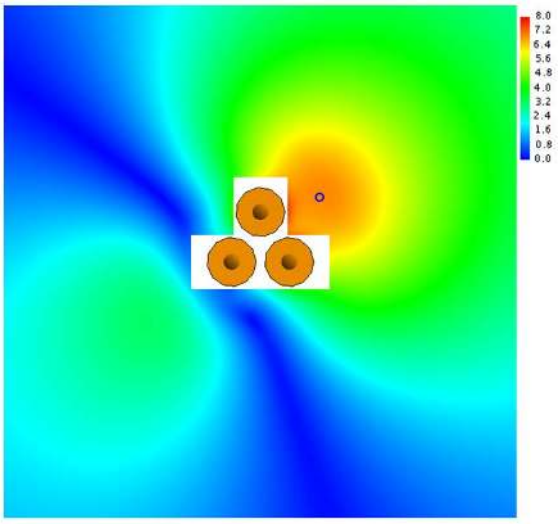

(b)

Fig.7. Retrodirection of the near field radiated by a Hertzian dipole source. (a) a vertical Hertzian dipole source of 1mAm amplitude is shown by the red arrow and is located at (0.24λ, 0.24λ,0.0); (b) retrodirected field $|E_z|$ radiated by a 3-element PC array, with the Hertzian source removed. Blue hollow dot shows the position of the Hertzian source.

The choice of a Hertzian dipole as a source of evanescent spectrum can be justified by the fact that the Hertzian dipole generates the illumination field and is not EM coupled to the resonance antenna array. Therefore a point-like source can be removed in the retrodirection mode without affecting the array near field properties. In a series of simulations the Hertzian source was positioned in the horizontal plane at the points $\rho_d \exp(i\varphi_d)$, where ρ_d varied from 0.2λ to 0.4λ and φ_d varied from 0 to 90 degrees with 30 degrees step.

In all cases the maximum of the retrodirected field (except for the vicinity of the antennae surfaces where the *E*-field is intrinsically high) was obtained in the illuminating dipole positions, Fig.7(b). Fig.7(b) also reveals the formation of the "negatively refracted" field, left bottom corner of the graph in Fig.7(b), in the mirror symmetric position with respect to the array which is fully consistent with the previous analysis.

The considered features of the near field in the PC array environment have utmost importance for the retrodirection properties of the PC array in the far field. As shown in the Appendix A, the antennae currents contain the DoA information encoded in both the propagating and the evanescent field. Since for compact antenna terminals the evanescent field amplitude can substantially exceed the amplitude of the incident propagating PW the retrodirection of the evanescent spectrum in the array environment plays a dominant role in the array excitation vector formation on transmit. The appearance of the "negatively refracted" spot creates an excitation to the array antenna elements which corresponds to the arrival of a spurious PW in the direction of negative refraction and leads to deterioration of the radiation pattern in the desired DoA direction. This effect will be further studied below.

It should be noted that the process of evanescent-to-propagating spectrum conversion and the reverse process of the propagating-to-evanescent field conversion leading to the extraction of the radiation system subwavelength features has been studied theoretically and experimentally in [20], [31]-[34]. It should be noted that in this paper we establish, for the first time, a complete EM picture of the retrodirected near field formation in ultra-compact antenna arrays using electrically small elements at high radiation efficiency which is crucial for free-space far-field wireless applications.

IV. Retrodirective Antenna Array Performance Considerations

A parametric study of the electrically small retrodirective antenna array performance as a function of array geometry is carried out in this Section. Particularly the effect of inter-element separation on the available gain and antenna element matching is discussed. Also the effect of the lattice geometry on beam pointing accuracy is studied with the emphasis of the near field coupling between the antennas and spatial coherence of the retrodirected near field. Finally a sensitivity analysis is carried out.

A. Gain and antenna matching bandwidth vs inter-element spacings

It is well known [5] that reduction of the antenna array inter-element spacing leads to lower antenna radiation resistance and hence lower available directional gain and smaller return loss (antenna matching) bandwidth. Possible solutions include modification of the antenna element geometry [35] and impedance, particularly resistive, loading across the antenna terminals [36]. In general, both the antenna geometry modification and resistive loading improve the antenna matching bandwidth at the expense of the antenna array available gain. In the present paper we restrict the analysis by considering only disk-loaded dipole antenna elements which ensure a uniform electric current maximizing the available gain [5].

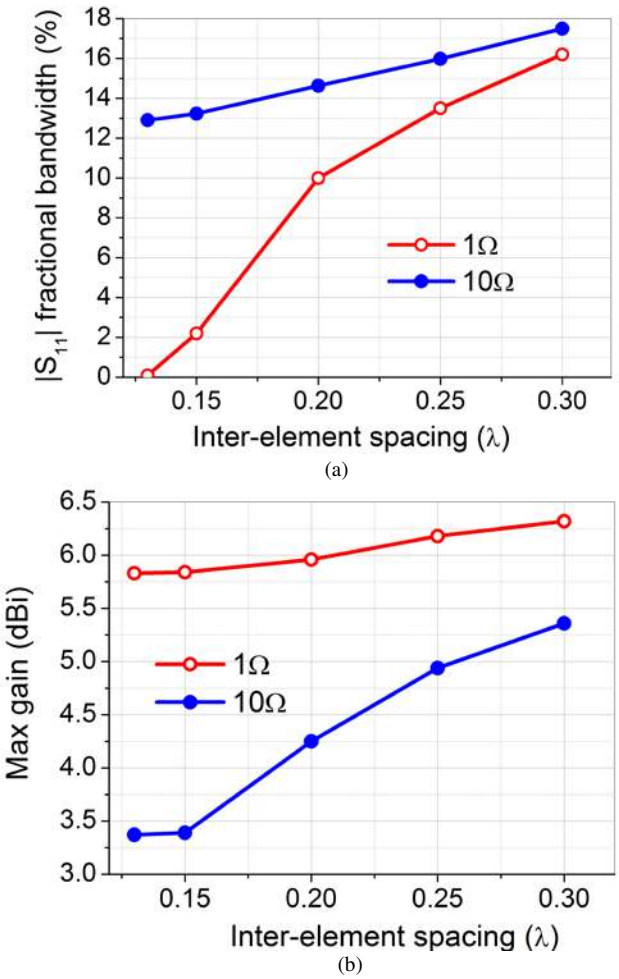

Fig.8. (a) Return loss, $|S_{11}|$ fractional bandwidth and (b) maximum gain at the DoA for the antenna terminal loading of 1Ω and 10Ω. The graphs are plotted for 3-element array with equilateral triangular lattice. (b) corresponds to the DoA (0,30°).

Fig. 8(a) shows simulated antenna return loss fractional bandwidth as a function of the inter-element spacings in the disk-loaded dipole array with equilateral triangular lattice. The antennae are fed via 50Ω port. It can be seen that even moderate increase of resistive loading leads to more than 10% matching bandwidth. At the same time antennae with very small 1Ω loading fail to operate at dense spacings less than 0.15λ. It should be noted that due to the resonance nature of the antenna elements, the radiation gain in the direction of the radiation pattern maximum can be reduced with increased resistive loading, Fig. 8(b), therefore a trade-off between the desired antenna matching bandwidth and available gain needs to be chosen. Another possibility is to design the antenna elements with high radiation resistance in free space, such that the reduction of the radiation resistance in the array environment could be less pronounced [10], this will be studied in future work.

B. Effect of array lattice geometry on the radiation pattern

The array lattice geometry affects the retrodirected pattern via two principal mechanisms.

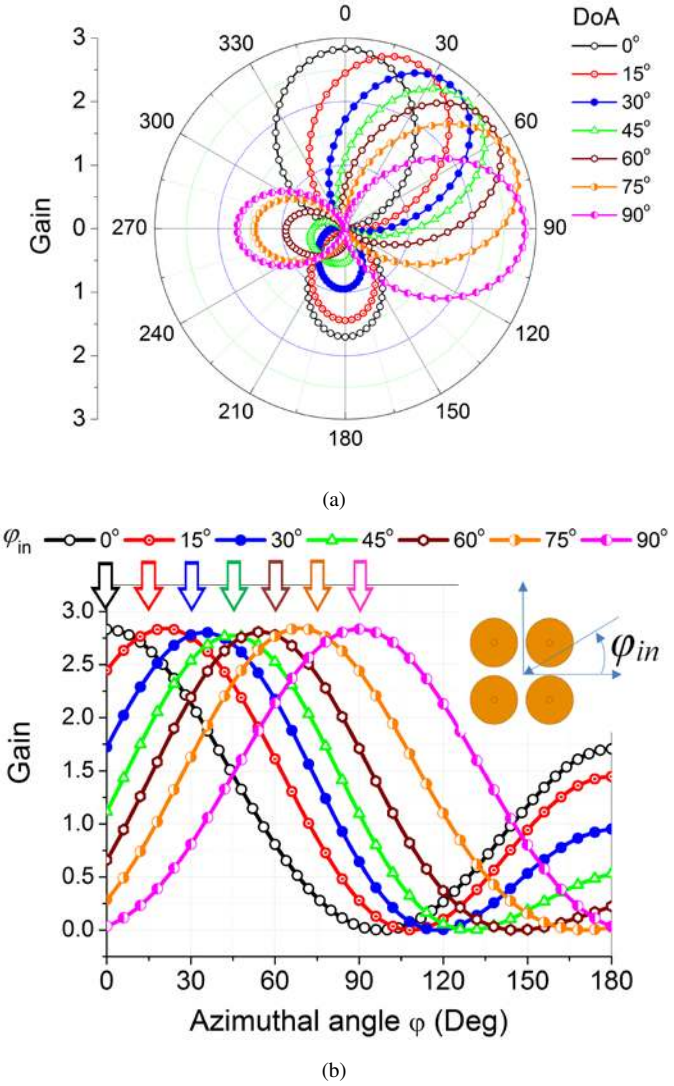

Fig.9. Retrodirection pattern of the 4-eement top-loaded dipole array arranged in a square lattice with 0.15λ spacings, antenna terminal load is 10Ω. (a) Full 360° azimuthal range; (b) 0-180° angular range in the radiation sector of the main lobe. DoA is shown by an arrow of the corresponding color.

First; in the lattices with uneven spacing radiation gain experiences variation with the scan angle which is however not substantial (less than 1dB) for moderate spacings variations (100% or less). Another potential source of the retrodirective array radiation pattern degradation is due to the inevitable appearance of the negatively refracted field (11), (20) which creates a contribution into the array excitation vector corresponding to the spurious DoA from the "negative refraction" direction. This contribution can be minimized in dense equilateral lattices or many-element arrays, due to the spatial coherence of retrodirective field and incoherence of the negatively refracted field.

Fig. 9 demonstrates the example of a retrodirection pattern generated by a 4 element array arranged in a square lattice with 0.15λ spacings. Full 360° range polar plot is shown in Fig. 9a) and the limited range 0-180 ° Cartesian graph is provided in Fig.9b) to demonstrate the detail of the radiated beam main lobes. It can be seen that the retrodirected beam experiences a squint of around 7° towards the diagonal axis φ=45° for any

DoA except for the symmetry axes φ=0°, φ=45°, φ=90°. For an electrically small array this beam squint does not cause any appreciable gain deterioration due to the wide angular bandwidth of the radiation pattern (~90°). Further simulations, not presented here for brevity, show that, any spatially compact (2) arrangement of more than three retrodirective antenna radiators with arbitrary arrangement of antenna elements enables omnidirectional RX/TX coverage in the azimuthal plane with small variation (less than 1dB) of the maximal gain in the DoA direction.

C. Sensitivity analysis

In classical superdirective arrays theory [4], [26] the sensitivity of the array pattern to random variations in the antenna positions and excitation vector is characterized by the sensitivity factor [4]. This metric can be applied to the retrodirective antenna terminal sensitivity characterization, however it should be remembered that classical superdirective arrays and retrodirective antenna terminals have a principal difference in operation. The excitation vector of a classical superdirective array is formed by the array polynomial roots which can be chosen arbitrarily in the complex plane to control the radiation pattern [26].The array radiation pattern error appears as a result of the difference between the computed/modelled antenna element positions/radiation properties and the actual ones. In the retrodirective antenna terminals the array excitation vector is electromagnetically set by the incident PW through the analog circuitry operation. If the propagation environment and array configuration do not experience abrupt temporal changes, retrodirected beam pointing error can only be caused by the amplitude or phase error in the PC circuitry.

To analyze this situation we consider first a 3-element disk-loaded dipole array with 0.15λ spacings and 10Ω resistive loading across the antenna terminals. It can be expected that due to relatively large angular bandwidth of the retrodirected beam (~90°) even substantial PC phase error at the output of a single antenna port in the radiating triplet should not appreciably affect the retrodirective antenna array performance. To confirm this, a series of simulations has been run with absolute phase error 10 to 40 degrees at the PC unit output of a single antenna element. The PC error at other two antenna elements was set to 0 degrees. Fig. 10(a) demonstrates the situation when 20° phase error is present across the terminals of the first element in the 3-element array. It can be seen that only minor deterioration of the radiation pattern is present (with beam squint error not exceeding 7 degrees and gain reduction less than 0.5dBi).

Next, the situation is modelled when the PC unit in the first element fails to operate and this antenna acts as a passive parasitic element. It can be seen, Fig. 10(b) that even in this case the PC array can retrodirect the beam in the range of DoA albeit with higher squint error (average 15°) and gain reduction. However for some DoA, viz. 180° in Fig.10(b) the PC array fails to retrodirect the beam in correct direction, orange line with triangular markers.

The retrodirective array performance deteriorates to higher extent when more than one PC units generate phase error. Simulation, not presented here for the brevity's sake, show that in the case of two and three antenna PC circuits generating 10° phase error the beam squint is no more than 5-7°. It should be noted that an average phase error in a high-performance PC unit normally does not exceed 5° [16].

Next, the simulations of multi-element retrodirective arrays with a number of elements more than three show that the multi-element arrays are quite insensitive to PC moderate phase errors (~ 10-40°) when sufficient number of elements operate correctly. Fig. 11(a) illustrates the situation when three elements out of six generate PC output with 20° phase error and three other elements perform PC with zero error. It can be seen that in this situation the beam pointing error is 5-7 degrees with the gain drop not exceeding 0.7dBi. Fig. 11(b) shows the retrodirected radiation pattern when two out of four antennae operate as passive parasitic elements. It can be seen that the PC array maintains retrodirection. However the gain significantly reduces (more than 1dBi) for certain DoA. Finally, the effect of the amplitude error at the output of PC unit on the retrodirected beam has been studied with the consequence that moderate variation of the PC voltage amplitudes (10-40%) does not adversely affect beam pointing accuracy and gain, therefore PC units with uniform amplitude output can be used. This should significantly simplify the PC hardware realization [16].

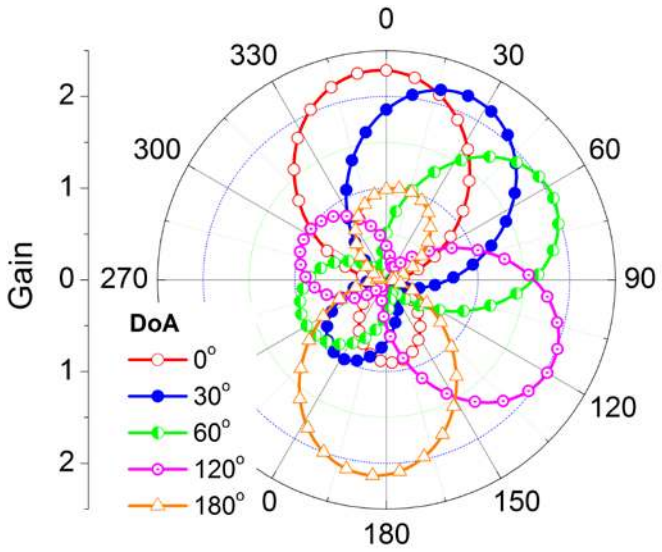

(a)

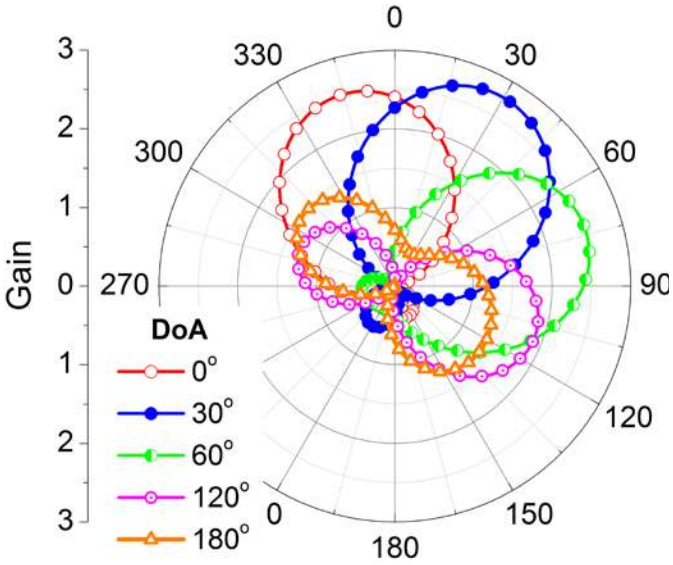

(b)

Fig.10. Retrodirected radiation pattern of 3-element disk-loaded dipole triangular lattice array with 0.15λ spacings. (a) The PC unit in the first element generates PC output with 20º phase error; (b) the first antenna operates as a passive parasitic element.

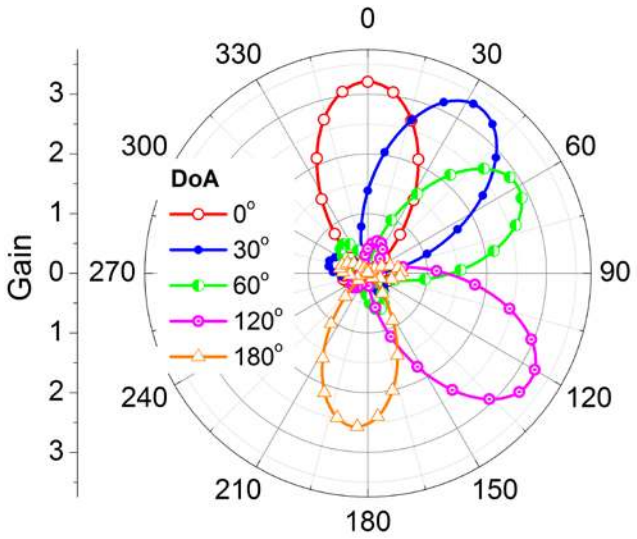

(a)

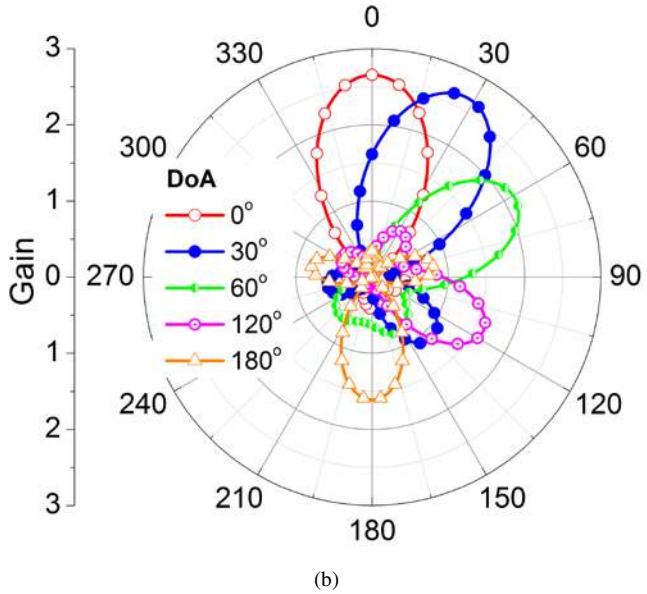

(b)

Fig.11. Retrodirected radiation pattern of the 6-element disk-loaded dipole circular array with 0.17λ radius. (a) The PC units in the first, third and fifth elements generate PC output with 20º phase error; (b) the second and forth antennae operate as passive parasitic elements.

V. CONCLUSIONS

In this paper we demonstrated that the DoA information carried by an incident EM wave can be encoded into the evanescent near field of an electrically small resonant antenna array with a spatial rate higher than the incident field spatial variation rate in free space. Phase conjugation of the received signal across the antenna terminals leads to the retrodirection of the near field in the antenna array environment which generates an antenna array far-field beam radiated towards the original DoA. This electromagnetic phenomenon enables electrically small retrodirective antenna arrays with superdirective, angular super-resolution, auto-pointing properties operating for arbitrary DoA in the azimuthal plane.

Full-wave simulations have been carried out to demonstrate practical realisability of the proposed retrodirective terminals comprised of resonance dipole antenna elements. Particularly it has been shown that 3-element disk-loaded dipole array arranged in a triangular lattice with 0.15λ spacings can achieve 3.4dBi maximal gain, 3dBi front-to-back ratio and 13% return loss fractional bandwidth. Next it is demonstrated that the radiation gain can be improved to approximately 6dBi at expense of the return loss fractional bandwidth reduction (2%). Finally, sensitivity analysis based on full-wave simulations, demonstrated that the proposed retrodirective terminals are free from the sensitivity issues pertinent to classical superdirective arrays. Moreover it is shown that multi-element retrodirective antenna arrays maintain their beam pointing action even if some of the antennae operate as parasitic elements after PC failure.

It is believed that the proposed antenna terminals could find applications in energy-efficient wireless communication systems and focused wireless energy transfer systems where space is a premium.

APPENDIX A.

This Appendix provides more detail of the EM scattering and re-radiation by a retrodirective antenna array. For simplicity let us consider straight antenna elements with electric current $I_n(z)$ variation along the z axis.

A. Antenna array in the receive mode

The current distribution $I_n(z)$ along the axis of the n-th antenna element is governed by the *Hallen's* equation [30], [37]

$$\int_0^{Ln} K(z,z')I_n(z')dz' = P_n(z) \tag{A1}$$

where the kernel $K(z,z')$ is a linear combination of the spherical wave functions [37] and the right hand side function $P_n(z)$ contains the projection of the total impingent electric field on the n-th antenna surface,

$$P_n(z) = \frac{Y_0}{2}\left[\Psi(z) + \alpha(z)\Psi(0) + \beta(z)\Psi(L_n)\right], \tag{A2}$$

$$\Psi(z) = \int_0^{L_n}\left[\vec{E}_{in}(\vec{r}') + \sum_{j,j\neq n}^{N}\vec{E}_{sc}^{(j)}(\vec{r}')\right]\cdot\vec{z}_0\exp\left(ik_0|z-z'|\right)dz' \tag{A3}$$

In (A2) Y_0 is the admittance of free space and the functions $\alpha(z)$, $\beta(z)$ are linear combinations of the harmonic term $\exp(ik_0 z)$. Equation (A1) arises as a consequence of the boundary condition stating that the total tangential E-field is zero at the metal surface. From (A3) it can be seen that the RHS excitation term can be written as a sum of two terms, $\Psi_{in}(z)+\Psi_{sc}(z)$, with the term Ψ_{in} containing the incident PW field only and the second term, Ψ_{sc}, which involves the total scattered field from all antennas except the n-th one. The term Ψ_{in} can be represented as

$$\Psi_{in}(z) = \Phi_n\int_0^{L_n}\vec{e}_{in}\cdot\vec{z}_0\cdot\exp(ik_0 z'\cos\theta_{in})\exp\left(ik_0|z-z'|\right)dz' \tag{A4}$$

where

$$\Phi_n = \exp\left(i\vec{k}_{in}\cdot\vec{\rho}_n\right) \tag{A5}$$

is the phase of the incident PW at the n-th antenna center at $\vec{\rho} = \vec{\rho}_n$. Suppose that the current distributions $I_n(z)$ are expanded into the Method-of-Moments (MoM) basis functions set $f_M^{(k)}$

$$I_n(z) \approx \sum_k \tilde{I}_n f_M^{(k)}(z) \tag{A6}$$

and (A1) is projected on this set. Then the solution column-vector $\underline{\underline{I}}_M$ for the current coefficients can be written in matrix form

$$\left[\underline{\underline{I}}_M\right] = \left[\underline{\underline{K}}_M - \underline{\underline{\tilde{P}}}_M^{(sc)}\right]^{-1}\cdot\left[\underline{\underline{\Phi}}\right]\cdot\left[\underline{\underline{\tilde{P}}}_M^{(in)}\right] \tag{A7}$$

In (A7) matrix $\underline{\underline{\Phi}}$ is a diagonal matrix with complex numbers Φ_n equal to the phase of the incident PW at the n-th antenna center (A5), and the diagonal matrices $\underline{\underline{\tilde{P}}}^{(in)}$, $\underline{\underline{\tilde{P}}}^{(sc)}$ are comprised of the incident and scattered field (A2)-(A4) MoM projections respectively. In (A6) $\underline{\underline{K}}_M$ is a matrix MoM projection of the left hand side of equation (A1).

The equation (A7) demonstrates that the DoA information contained in matrix $\underline{\underline{\Phi}}$ is encoded into the antenna current distributions $I_n(z)$ via the propagating incident PW, $\underline{\underline{\tilde{P}}}^{(in)}$ and scattered field in the antenna array environment, $\underline{\underline{\tilde{P}}}^{(sc)}$.

B. Antenna array in the retrodirection mode

A voltage drop v_n induced across the n-th antenna terminal at $z = z_n^{(t)}$ by the incident PW can be written as a product of the current distribution in the receive mode $I_n(z)$ and linear part of the antenna terminal Z_{Ln},

$$v_n = I_n\left(z_n^{(t)}\right)Z_{Ln} \tag{A8}$$

It can be seen from (A7), (A8) that phase conjugation of the complex-valued voltage (A8) leads to propagating wavefront reversal, $\sim\exp\left(i\vec{k}_{in}\cdot\vec{\rho}_n\right)$ at the antenna elements and the near field retrodirection in the antenna array environment. The resulting phase conjugated field is given by (14) where the current amplitudes can be found from the MoM matrix equation [37] with excitations (A8) analogous to (A7).

APPENDIX B

The spectral amplitudes of the PW expansions in (17) are given by

$$\vec{\mathrm{E}}(\vec{k}) = \left(\frac{k_0\vec{z}_0}{k_z} - \frac{\vec{k}}{k_0}\right), \tag{A9}$$

$$k_z = \sqrt{k_0^2 - k_x^2 - k_y^2}$$

REFERENCES

[1] A.J. Goldsmith, Wireless Communications, Cambridge University Press, 2005.

[2] S. Saunders, A. Aragón-Zavala, Antennas and Propagation for Wireless Communication Systems, Wiley 2007.

[3] Pak Chan, V. Fusco, "5.8 GHz full duplex amplitude shift keying retrodirective interrogator array", *Microwave Optical Technology Letters,* vol. 55, no.1, pp. 160-164, Jan. 2013.

[4] E. H. Newman, J.H. Richmond, C. H. Walter, "Superdirective receiving arrays," *IEEE Trans. Antennas Propagat.,* vol. AP-26, no.5, pp. 629 - 635, Sept 1978.

[5] R.C. Hansen, R. E. Collin, Small Antenna Handbook, John Wiley & Sons, Inc. 2011.

[6] K. Fujimoto, A. Henderson, K. Hirasawa, and J. R. James, Small Antennas, Wiley, 1987.
[7] H. Yagi, "Beam transmission of ultra short waves", *Proceedings IRE*, vol. 16, pp. 715-741; June,1928.
[8] W. Ehrenspeck and H. Poehler, "A New Method for Obtaining Maximum Gain from Yagi Antennas", *IRE Trans. Antennas Propagat*. Vol. 7, no. 4, pp. 379-386, 1959,
[9] A. D. Yaghjian, T. H. O'Donnell, E. E. Altshuler, and S. R. Best, "Electrically small supergain end-fire arrays", *Radio Science*, vol. 43, RS3002, pp1-13, 2008.
[10] Altshuler, E. E., T. H. O'Donnell, A. D. Yaghjian, and S. R. Best, "A monopole superdirective array", *IEEE Trans. Antennas Propag*., vol. 53, no. 8, pp. 2653–2661, Aug. 2005.
[11] R.W.P. King, "Supergain Antennas and the Yagi and Circular Arrays", *IEEE Trans Antennas Propagat*., vol.37, no.2, pp. 178-186, Feb.1989.
[12] H.-T. Liu, S. Gao, and T.-H. Loh, "Electrically Small and Low Cost Smart Antenna for Wireless Communication", *IEEE Trans. Antennas Propagat.*, vol.60, no.3, pp. 1540-1549, March 2012
[13] H.-T. Liu, S. Gao, and T.-H. Loh, "Compact MIMO Antenna With Frequency Reconfigurability and Adaptive Radiation Patterns", *IEEE Trans. Antennas Propagat. Lett.*, vol. 12, pp. 269-272, 2013.
[14] Y. Zhou, R. S. Adve, Sean Victor Hum, "Design and Evaluation of Pattern Reconfigurable Antennas for MIMO Applications", *IEEE Trans. Antennas Propagat.*, vol.62, no.3, pp. 1084-1092, March 2014.
[15] C. Sun, A. Hirata, T. Ohira, N. Karmakar, "Fast Beamforming of Electronically Steerable Parasitic Array Radiator Antennas: Theory and Experiment", *IEEE Trans. Antennas Propagat.*, vol.57, no.7, pp. 1819-1832, July 2004.
[16] V. Fusco, N. Buchanan, "Developments in retrodirective array technology", *IET Microw. Antennas Propagat*., , vol. 7, no. 2, pp. 131–140, 2013.
[17] R.C. Hansen, "Fundamental limitations in antennas", *Proceedings IEEE*, vol. 69, no.2, pp. 170-182, Feb. 1981.
[18] O. Malyuskin, V. Fusco, A. Schuchinsky, "Microwave phase conjugation using nonlinearly loaded wire arrays", *IEEE Trans. Antennas Propagat.*, vol.54, no.1, pp. 192-203, 2006.
[19] K.M.K.H. Leong, Y. Wang, T. Itoh, "A full duplex capable retrodirective array system for high-speed beam tracking and pointing applications", *IEEE Trans. Microwave Theory Techniques*, vol.52, no.5, pp. 1479-1489, 2004.
[20] V. Fusco, O. Malyuskin, N. Buchanan, "Active phase conjugating lens with sub-wavelength resolution capability", *IEEE Trans. Antennas Propagat.*, vol.58, no.3, pp. 798-808, 2010.
[21] R. Mailloux, Phased Array Antenna Handbook, 2nd ed. Norwood, MA, USA: Artech House Antenna Library, 2005.
[22] K. Buell, H. Mosallaei and K. Sarabandi, "Metamaterial Insulator Enabled Superdirective Array", *IEEE Trans. Antennas Propagat.*, vol. 55, no.4, pp. 1074-1085, 2007.
[23] T.B. Hansen, A.D. Yaghjian, Plane-Wave Theory of Time-Domain Fields : Near-Field Scanning Applications, Wiley IEEE, 1999.
[24] L. M. Brekhovskih, Waves in Layered Media, Academic Press, 1980.
[25] O. Malyuskin, V. Fusco, "Near field focusing using phase conjugating impedance loaded wire lens", *IEEE Trans. Antennas Propagat.*, vol. 58, no.9, pp. 2884-2893, 2010.
[26] S.A. Schelkunoff, "A Mathematical Theory of Linear Arrays", *Bell Syst. Tech. Journal*, vol. 22, pp. 80-107, 1943
[27] J. Capon, "High-resolution frequency-wavenumber spectrum analysis", *Proceedings IEEE*, vol. 57, pp.1408-1418, Aug. 1969.
[28] H.A. Wheeler, "The radian sphere around a small antenna", *Proc. IRE,* vol. 47, pp. 1325-1331, 1959.
[29] E.V. Jull, Aperture Antennas and Diffraction Theory, Peter Peregrinus, 1981. Chapter 5.
[30] L. Chen, Y. C. Guo, X. W. Shi, and T. L. Zhang, "Overview on the Phase Conjugation Techniques of the Retrodirective Array", *Int. Journal Antennas Propagat*., vol. 2010, pp.1-10, Article ID 564357, doi:10.1155/2010/564357.
[31] J.-W. Tsai, C.-H. Wu,T.-G. Ma, "Novel Dual-Mode Retrodirective Array Using Synthesized Microstrip Lines", *IEEE Trans. Microwave Theory Tech.* vol. 59, no.2, pp. 3375-3388, 2011.
[32] C. Balanis, Antenna Theory. Chapter 2. Wiley & Sons, 1997.
[33] J.A. Kong, Electromagnetic Wave Theory, EMW Publishing, 2000.
[34] O. Malyuskin, V. Fusco, "Far field subwavelength source resolution using phase conjugating lens assisted with evanescent-to-propagating spectrum conversion", *IEEE Trans. Antennas Propagat.*, vol. 58, no.2, pp. 459-468, 2010.
[35] M. Nieto-Vesperinas and E. Wolf, "Phase conjugation and symmetries with wave fields in free space containing evanescent components," *J. Opt. Soc. Amer*., vol. 2, no. 9, pp. 1429–1434, 1985.
[36] R. Carminati, J. J. Sáenz, J.-J. Greffet, and M. Nieto-Vesperinas, "Reciprocty, unitarity and time-reversal symmetry of the S matrix of fields containing evanescent components," *Phys. Rev. A*, vol. 62, pp. 012712–012712, 2000.
[37] G. Lerosey, J. de Rosny, A. Tourin, and M. Fink, "Focusing beyond the diffraction limit with far-field time reversal," *Science*, vol. 315, pp. 1120–1120, 2007.
[38] S. Best, "The performance properties of electrically small resonant multiple-arm folded wire antennas", *IEEE Antennas Propag. Mag*., vol. 47, pp. 13–27, 2005.
[39] Kraus, J. D., and R. J. Marhefka , Antennas, 3rd ed., McGraw-Hill, New York, 2001.
[40] O. Malyuskin, V. Fusco, A. Schuchinsky, "Modelling of impedance-loaded wire frequency-selective surfaces with tunable reflection and transmission characteristics", *Int. Journal of Numer. Modelling: Electronic Networks, Devices and Fields*, vol. 21, pp. 439-453, 2008.
[41]